THE AMERICAN SOCIETY OF MECHANICAL ENGINEERS
345 E. 47th St., New York, N.Y. 10017

96-GT-263

EFFECT OF CIRCUMFERENTIAL INLET FLOW DISTORTION AND SWIRL ON THE FLOW FIELD OF AN AXIAL FLOW FAN STAGE

K. Viswanath and M. Govardhan
Thermal Turbomachines Laboratory
Department of Mechanical Engineering
Indian Institute of Technology, Madras 600 036, India

ABSTRACT

This paper reports a study of the combined effects of swirl and circumferential inlet flow distortion on the flow field of an axial flow fan stage. The study involves steady state measurements of the flow field at the rotor inlet, exit and the stator exit of the single stage axial flow fan subjected to circumferential inlet flow distortion and swirl. Flow field survey was done at two flow coefficients, namely, $\phi = 0.45$ and $\phi = 0.285$. The flow at the inlet to the rotor was measured using a three hole pressure probe and five hole pressure probes were used at the rotor and stator exits. The study indicated that at the design flow coefficient swirl had caused deterioration of the performance in addition to that caused by distortion. In addition, the attenuation of distortion was high in the presence of swirl.

NOMENCLATURE

C.I.	clean inlet
C_m	meridional velocity
D.M.	distortion mesh
D_t	tip diameter of the rotor
N_c	input power to the fan
N_{eff}	effective fluid power $N_{eff} = V(P_{o3} - P_{o1})$
P_{coeff}	power coefficient $P_{coeff} = 2N_c/(\rho\pi D_t^2 U_t^3)$
P_o	total pressure
R	non-dimensionalised radius ratio
S.M.	support mesh
U_t	rotor tip speed
V	flow rate
ϕ	flow coefficient $\phi = C_m/U_t$
γ	stagger angle of the IGV blades
η	efficiency of the stage $\eta = N_{eff}/N_c$
ρ	density of air
ψ	energy coefficient $\psi = 2(P_{o3}-P_{o1})/\rho U_t^2$

Subscripts

1	inlet to rotor
2	exit of rotor
3	exit of stator

INTRODUCTION

Inlet flow distortion is a term used to denote the variation of flow properties as a function of the spatial co-ordinates and time. The non-uniformity occurs in common flow properties such as total pressure, static pressure, velocity, temperature, flow angle and gas constituency. Swirl is the term used to describe the rotation of flow in relation to the rotation of the rotor. Swirl may be generated as a consequence of secondary flows induced due to flow curvatures or due to the presence of IGV. Distortion and Swirl (induced due to curvature of flow passages) cause a decrease in pressure ratio, corrected mass flow and efficiency. They also tend to cause premature compressor stall and, due to fluctuating blade forces, there is a possibility of blade vibration and blade failure. Flow distortions are classified as circumferential or radial depending on the orientation of the defect. Circumferential distortions are caused by non-axisymmetric defects such as the existence of separated flow regions, wakes from the upstream blade rows, etc. In many cases and under certain operating conditions, the inlet flow will exhibit either, or both, circumferential and radial non-uniformities.

Swirl is categorised into bulk swirl and twin swirl (Aulehla, 1982). Swirl can be regarded as co-rotating and counter-rotating swirls when related to the rotation of the rotor. A counter-rotating swirl can trigger surging of the engine. The aerodynamic performance of a compressor depends on the relative magnitude of one swirl with respect to the other. Total pressure distortion and swirl distortion have been identified as the two major intake engine compatibility parameters. Of these, swirl has been identified to play an important role, as conceived during the flight testing of the Tornado aircraft (Aulehla,1982). The problem of angular swirl at the engine face, induced due to flow curvatures, has come to the fore in

Presented at the International Gas Turbine and Aeroengine Congress & Exhibition
Birmingham, UK — June 10-13, 1996

the recent years. Extensive work has already been done on the study of circumferential distortions. The present investigations consider the combined effects of swirl and circumferential distortion.

Most of the literature available till date on inlet flow distortion deals extensively on circumferential distortion alone (Colpin, 1979; Ehrich, 1957; Yocum and Henderson, 1980) and only recently few investigators have considered the combined effects of swirl and circumferential distortion. Flitcroft et al. (1987) investigated the effect of inlet swirl on the propagation of total pressure distortion through a 3-stage fan without IGV. They found that the presence of a swirl counter to the rotation of the fan generally reduced the level of steady state distortion transmitted to the core compressor. Pazur and Fottner (1991) studied the influence of swirl distortions on the low pressure compressor of a two spool turbofan Larzac 04 engine. The measured performance map was compared with the computed performance map with distorted inflow having co-swirl and counter swirl. The comparison showed shifting of constant speed lines to lower pressure ratios as well as to lower mass flow rates. The surge line was shifted resulting in a lower surge margin than that for undistorted flow. The isentropic efficiency was also found to be smaller for distorted flow.

The aim of the present investigations is to study the effect of swirl and circumferential distortions on the performance degradation of an axial flow fan stage and the attenuation and amplification characteristics of the defect. A combination and swirl and distortion would occur when a separated inlet flow has to pass through curved inlet ducting. The study includes (i) steady state measurements at inlet and exit of the rotor and at downstream of the stator (ii) the effects of varying the flow coefficients on the flow field.

EXPERIMENTAL FACILITY AND TECHNIQUE

A schematic layout of the axial flow fan test rig used for the present investigations is shown in Fig. 1. The axial flow fan stage comprised of a six bladed forced vortex rotor followed by an eight bladed stator. The design data of the impeller is furnished below:

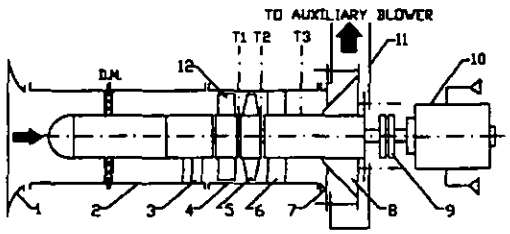

1. Inlet nozzle 2. Inlet duct 3. Radial supports 4. Impeller housing 5. Rotor 6. Stator 7. Discharge nozzle 8. Throttle cone 9. Coupling 10. D.C. Drive motor 11. Discharge casing 12. IGV T. Measuring planes D.M. Distortion mesh

Fig. 1 Schematic Lay-out of Axial Flow Fan

Tip diameter, D_t = 250 mm; Hub diameter, D_h = 100 mm; No. of blades, Z = 6; Hub-tip ratio, D_h/D_t = 0.4; Inlet blade angle at hub, $\beta_{1h} = 51.3^0$; Outlet blade angle at hub, $\beta_{2h} = 72.3^0$; Inlet blade angle at tip, $\beta_{1t} = 26.6^0$; Outlet blade angle at tip, $\beta_{2t} = 47.6^0$; Solidity at hub σ_h = 0.96; Solidity at tip σ_t = 0.53; Speed = 4500 rpm; Vortex condition = Forced vortex flow: $C_u r^{-0.65}$ = constant.

The outlet of the axial flow fan was connected to an auxiliary radial blower to augment the decrease in mass flow rate when the flow was distorted. Provision was made for the measurement of the flow field at the inlet and exit of the rotor and downstream of the stator. The fan was run by a 10 KW DC dynamo motor. The cambered IGV blade section is derived from NACA 65-(12)10. These blades were not twisted and 6 blades were employed.

Distortion was generated using a perforated screen of 120^0 extent (with a porosity of 0.84) fixed to a support mesh and placed at a distance of 470 mm upstream of the rotor leading edge (about 1.9 times D_t). From the literature available, the location of the screen with respect to the rotor leading edge was found to be in the range of 1.5 to 2.5 times D_t. This had to be taken into account in order to isolate the screen from the rotor, since it is well known that a rotor will strongly alter the upstream flow when the flow is non-uniform. Swirl was varied by adjusting the stagger of the IGV blades. Typical configurations are shown in Fig. 2.

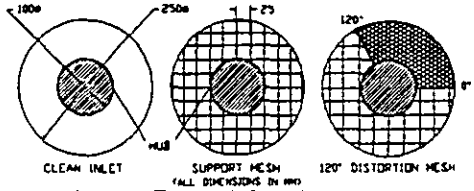

Fig. 2 Typical Configurations

Inlet flow to rotor was measured with a three hole pressure probe in non nulling mode. At the rotor and stator exits, the measurements were done using two miniaturised five hole pressure probes. The experiments were carried out for 4 different configurations. Configuration 1: The case of distortion without IGV; Configuration 2: The case of distortion with IGV at 0^0 stagger; Configuration 3: The case of distortion with IGV at -10^0 stagger; Configuration 4: The case of distortion with IGV at 5^0 stagger.

For all the above configurations flow field investigations for clean inlet and support mesh cases were also carried out: The data thus described was obtained for two flow coefficients, namely, ϕ = 0.45 and ϕ = 0.285. These flow coefficients were determined from the clean inlet 'ϕ - ψ' characteristic of the fan, Fig. 3. ϕ = 0.45 corresponds to the maximum specific work and ϕ = 0.285 corresponds to an operating point which penetrated sufficiently into the stall region. To make measurements circumferentially, the mesh was rotated relative to the probes which were kept fixed. Data for the distortion configurations was obtained at 17 circumferential locations. For each location the probes were traversed radially from hub to tip through 15 radial stations covering the annulus height of 75 mm. Care was taken to capture the data more closely near the hub and tip walls and also in the region of distortion. The pressures were recorded on a digital micro-manometer through a 20 channel scanning box. Data reduction was done with the help of a computer programme. The performance tests for all the clean inlet and support mesh cases were determined by running the machine at a constant speed of 4500 rpm and varying the flow rate.

RESULTS AND DISCUSSION

Typical variations of total pressures are presented here in the form of circumferentially averaged plots and contour plots. In the circumferentially averaged plots the total pressures for the distortion configurations are circumferentially mass averaged and plotted against 'R'. Unless and otherwise mentioned the contour plots presented here are for the configurations without IGV and with IGV

at 5° stagger. Pressures are non-dimensionalised with the dynamic head based on U_t. This is followed by a discussion on the performance estimates (η, ψ, P_{coeff}) and distortion indices. The bias and precision errors associated with the measurements were considered and the total uncertainties in the quantities presented here are as follows: $\pm$0.73% in the non-dimensionalised P_o and ψ, $\pm$0.42% in η and $\pm$0.76% in P_{coeff}.

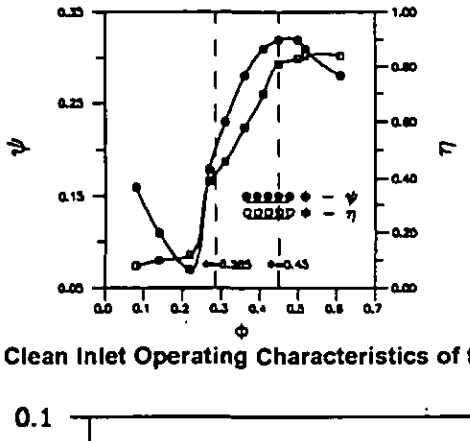

Fig. 3 Clean Inlet Operating Characteristics of the Fan

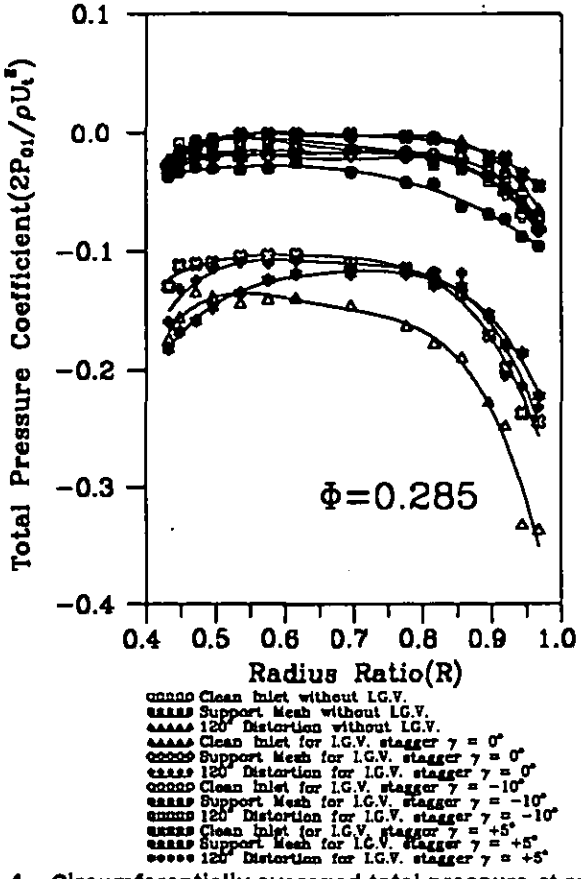

Fig. 4 Circumferentially averaged total pressure at rotor inlet

Rotor Inlet Total Pressure

As seen from the circumferentially averaged plots, Figs. 4 to 5, at the rotor inlet, the total pressure for clean inlet is uniform across the annulus except near hub and tip walls. The support mesh and clean inlet configurations differ slightly in the pressure distributions at the rotor inlet which is because of the resistance offered by the support mesh. In general clean inlet and support mesh configurations show higher pressures than that for the cases of distortion indicating the effect of distortion.

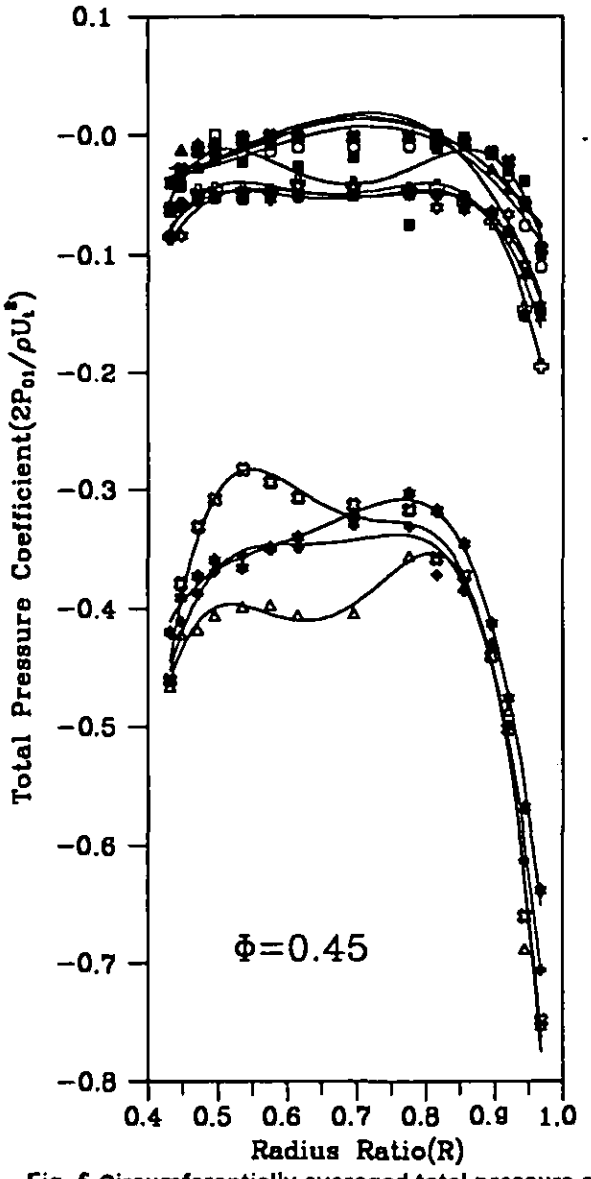

Fig. 5 Circumferentially averaged total pressure at rotor inlet (see Fig 4 for legend)

As seen in the contour plots for total pressure at rotor inlet, Figs. 6 to 7, the total pressure shows a wake type of defect in the distortion zone and registers an increase as one moves away from the distortion zone into the free zone. The total pressure decreases towards the walls suggesting the effect of wall boundary layers. The decrease in total pressure is high for the cases of distortion at the tip region as seen from both the contour plots as well as circumferentially averaged plots. The total pressures for the cases of distortion for ϕ = 0.45, Fig. 5, are lower than those for the cases of ϕ

= 0.285, Fig. 4, which is due to the fact that losses are proportional to volume flow rate. Swirl did not effect any redistribution in the total pressure at rotor inlet.

Fig. 6 Total pressure contours at rotor inlet (without IGV, ϕ = 0.45)

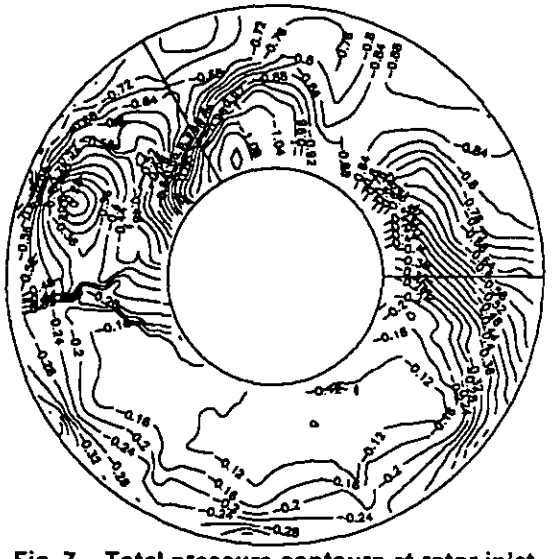

Fig. 7 Total pressure contours at rotor inlet ($\gamma = 5^0$, ϕ = 0.45)

Rotor Exit Total Pressure

At the rotor exit, for ϕ = 0.285, the circumferentially averaged total pressure profiles in Fig. 8 show variation among the cases of clean inlet and all configurations show a peak at the tip. This peak is due to the flow reversal taking place at the hub wall boundary layer at ϕ = 0.285. The blockage at the hub causes an increase in the flow velocities at the tip. In general, total pressure at rotor exit rises from hub to tip in conformity with the forced vortex design.

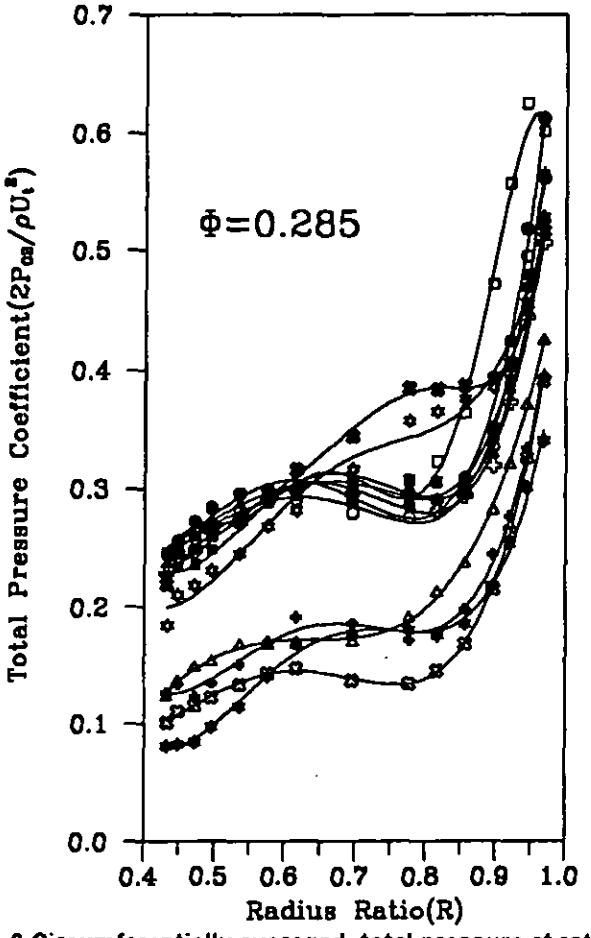

Fig. 8 Circumferentially averaged total pressure at rotor exit (see Fig 4 for legend)

Effect of distortion can be seen by comparing the distortion and clean inlet cases presented in the circumferentially averaged form. It can be seen that the circumferentially averaged pressures for the distortion cases are lower than those corresponding to the clean inlet cases, Figs. 8 and 9. For ϕ = 0.45, Fig. 9, the total pressure distributions for different cases seem to differ very much than that for ϕ = 0.285, Fig. 8. This indicates that for ϕ = 0.285 attenuation of almost the same extent is reached in all cases with distortion. Also attenuation as seen from the contour plots is more in the case of ϕ = 0.285, Figs. 10 to 11, where the defect persists only in the hub region. In these cases distortion attenuation is more evident in the midspan where there is almost equalisation of the pressure. For the cases of ϕ = 0.45 the defect seems to be present in the entire distortion zone with the distortion zone still showing pressures much lower than those in free zone, Fig 12. A comparison of rotor exit total pressure, Fig. 12, with the rotor inlet total pressure, Fig. 6, shows that the pressure rise imparted to the flow across the rotor is higher in distortion zone than that in the free zone. The less pronounced variations in the cases of ϕ = 0.285 are due to lower losses and better redistribution. As seen from circumferentially averaged plots for ϕ = 0.285, Fig. 8, the rise in pressure from hub to mid span is not much when compared to the rise in pressure at the tip. But for ϕ = 0.45 cases, Fig. 9, the circumferentially averaged plots show a fall in pressures at tip and hub sections. This is due to

the presence of low pressure, low velocity fluid at the inlet of this region, Fig. 7. The cause of the high gradient in the distortion zone, Figs. 10 to 13, can once again be attributed to the blockage at hub.

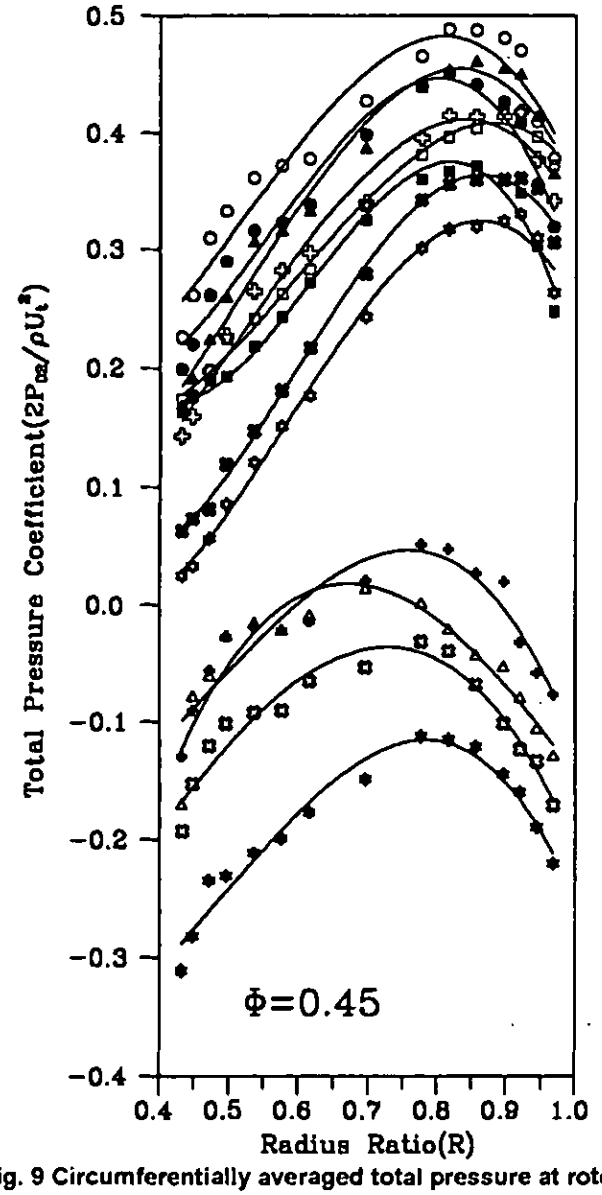

Fig. 9 Circumferentially averaged total pressure at rotor exit (see Fig 4 for legend)

The cases of clean inlet and support mesh for $\phi = 0.45$, Fig. 9, showed that the pressures are the highest for the case with IGV at -10^0 stagger indicating that the rotor blades can receive the flow at these incidences without stalling. The least pressures in the clean inlet, support mesh cases occur for the case with IGV at 5^0 stagger indicating the effect of swirl which is co-rotating in relation to the rotor rotation, Fig. 9. For the cases of clean inlet and support mesh without IGV and with IGV at 0^0 stagger, the distribution is intermediate of those mentioned earlier. The same trend does not continue for the cases with distortion, Fig. 9. It is seen that for the case of distortion with IGV at -10^0 stagger (i.e., swirl counter rotating with respect to the rotor rotation) the pressures were lower than those for the cases without IGV and with IGV at 0^0 stagger. This indicates that for the case of distortion with IGV at -10^0 stagger the low flow sector has penetrated well into the stall zone. As is expected for the case of distortion with IGV at 5^0 (i.e., with co-rotating swirl) the pressure distribution is below those of the remaining configurations.

Fig. 10 Total pressure contours at rotor exit (without IGV, $\phi = 0.285$)

Fig. 11 Total pressure contours at rotor exit ($\gamma = 5^0$, $\phi = 0.285$)

Stator Exit Total Pressure

The total pressure contours at stator exit show that the non-uniformity still persists at this station, Figs. 14 to 15. The non-uniformity appears to have reduced in magnitude as well as extent when compared to that at rotor inlet and exit. Also the total pressures are almost uniform in the radial direction.

A comparison of the stator exit total pressure with the rotor exit total pressure at both the flow coefficients would give information about the losses accompanying diffusion as the flow passes through the stator. These losses (P_{02} - P_{03}) are presented here for the case of IGV at -10^0 stagger for both the flow coefficients, Figs. 16 to 17. The rise in total pressure (negative values of the contours) in any region can be attributed to mixing and losses can be seen as a drop (positive values of the contours) in total pressure. It was observed from such a comparison that for all the cases of $\phi = 0.45$ the extent of regions registering drop in pressure was almost equal to the extent of regions of total pressure rise. This suggests that considerable amount of mixing has taken place for $\phi = 0.45$ with lower losses. In contrast to this, at $\phi = 0.285$ the regions of positive total pressure rise through the stator occurred around the hub region of the distortion zone. The remaining portion of the annulus showed total pressure drop and also the magnitudes of total pressure drop were higher in these regions than the magnitudes of total pressure rise which had occurred in the hub of distortion zone. The drop can be seen to be more in the tip region in general and is maximum in the tip region of the distortion zone. This can be attributed to the low axial velocities and high positive incidences of the flow at the inlet to the stator in those regions. The higher magnitudes of the total pressure drop and the considerable extent of region registering the drop suggests that the losses were very high for $\phi = 0.285$. The lower magnitudes of the total pressure rise and the lesser extent of the appearance of these regions suggest that there is no efficient mixing taking place through the stator at $\phi = 0.285$. Also the losses calculated from the mass averaged values were higher for $\phi = 0.285$.

Fig. 12 Total pressure contours at rotor exit (without IGV, $\phi = 0.45$)

Performance Characteristics of the Fan

The performance estimates for the cases of distortion, ψ and η, are based on the mass averaged total pressures obtained from the detailed flow field survey (which takes care of the non-uniformity in the flow). As the detailed flow field survey for the cases of distortion was done only at two flow coefficients, the overall characteristics for distortion configurations could not be determined for the entire clean inlet operating range. Hence the performance estimates, in Table 1(a), 1(b) and 1(c), for the cases of clean inlet, support mesh and distortion mesh are tabulated only for the two flow coefficients. Table 1(a) and Table 1(b) show the drop in the values of η and ψ for the case of distortion without IGV at $\phi = 0.45$ when compared with the corresponding clean inlet case. The reduction in the operating range was observed from the decrease in the throttle position. A reduction in ψ and η much higher than that mentioned above can be seen for the cases of distortion with the IGV at 5^0 and -10^0 stagger at $\phi = 0.45$. This indicates that the presence of swirl in addition to distortion is much more detrimental to the operation of the fan stage. The presence of a counterrotating swirl in addition to distortion causes part of the blading subjected to the low flow (due to distortion) to be pushed more into the stall zone thus causing further reduction in ψ and η. Similarly the presence of a co-rotating swirl in addition to distortion causes part of the blading subjected to the high flow to be operating under more negative incidences causing again a reduction in ψ and η. The additional degradation of the performance in the presence of counterrotating swirl was also observed by Flitcroft et al. (1987).

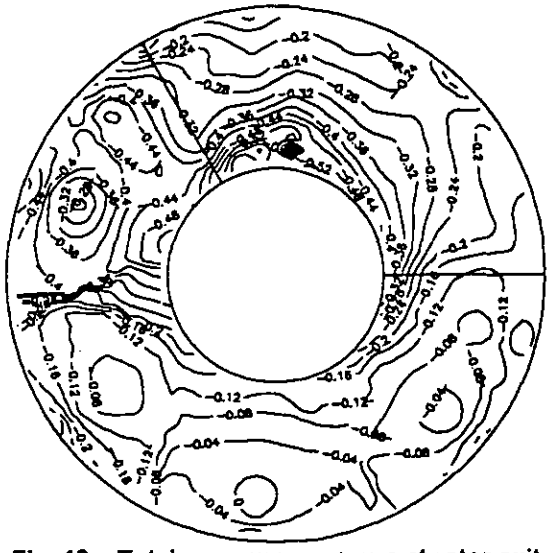

Fig. 13 Total pressure contours at rotor exit ($\gamma = 5^0$, $\phi = 0.45$)

The flow in both the free zone and distortion zone of the distortion configurations at $\phi = 0.285$ corresponded to the rising portions on either side of the dip which occurred in the clean inlet characteristics '$\phi - \psi$' (Fig. 3) and 'ϕ - P_{coeff}' (not shown here). The result is that there is an increase in the ψ and P_{coeff} at $\phi = 0.285$ in the presence of distortion. Similarly the presence of swirl in addition to distortion causes an additional shift and hence a difference among the various configurations at $\phi = 0.285$. It can also be seen that the variation in η with distortion at $\phi = 0.285$ is not similar to that of ψ and P_{coeff}. This can once again be attributed to the shape of the operating characteristics as follows. The clean inlet '$\phi - \eta$' characteristic (Fig. 3) is a rising characteristic over range tested. Both the clean inlet '$\phi - \psi$' and 'ϕ - P_{coeff}' characteristics contain a dip close to $\phi = 0.285$.

Fig. 14 Total pressure contours at stator exit (without IGV, ϕ = 0.45)

Fig. 15 Total pressure contours at stator exit ($\gamma = 5^0$, ϕ = 0.45)

Distortion Index

To judge both the quality of the intake flow and the tolerance of the fan a Distortion Index used in the present study is defined as follows.

$$DC(\theta) = (P_{of} - P_{o\theta})/q_f$$

where P_{of} is the mean total pressure at the measurement plane, q_f is the corresponding mean dynamic head and $P_{o\theta}$ is the mean total pressure in the worst sector of the plane. In the present investigations DC(120) is used to estimate the distortion index.

Distortion indices at the 3 locations for all the cases of distortion at both the flow coefficients are presented in Table 2. Distortion index is high at the rotor inlet. At the rotor exit there is a reduction in the distortion index at both the flow coefficients indicating that the effect of the rotor is to attenuate the distortion. At the rotor exit the index for the cases of ϕ = 0.45 is higher than that for ϕ = 0.285. This was already evident from the total pressure contours at the rotor exit for ϕ = 0.45 which have shown that the defect persists in the entire distortion zone. For ϕ = 0.285 the distortion index has dropped to a negative value which is attributed to the shifting of the defect from the tip region into the free zone. The lower value of the index for ϕ = 0.285 at the rotor exit could be attributed to the better redistribution due to the steepness of the performance characteristic at this operating point.

Fig. 16 Total pressure loss across stator ($\gamma = -10^0$, ϕ = 0.285)

Fig. 17 Total pressure loss across stator ($\gamma = -10^0$, ϕ = 0.45)

At the stator exit the defect has amplified for all the cases of ϕ = 0.285 which is because of the increased losses in the stator row.

The distortion indices for the cases of $\phi = 0.45$ at stator exit are lower than those for $\phi = 0.285$ indicating that the overall attenuation for the entire fan stage was higher for $\phi = 0.45$. For both the flow coefficients the attenuation at the stator and rotor exit was higher in the presence of swirl which can be attributed to the increased fluctuation in incidences to which the rotor is subjected. The increased attenuation of distortion in the presence of a counterrotating swirl was also observed by Flitcroft et al. (1987).

Table 1a. 'η' for various configurations.

	C. I. $\phi = 0.45$	S. M. $\phi = 0.45$	D. M. $\phi = 0.45$	C. I. $\phi = 0.285$	S. M. $\phi = 0.285$	D. M. $\phi = 0.285$
Without IGV	0.81	0.80	0.70	0.39	0.39	0.46
With IGV ($\gamma = -10^0$)	0.75	0.81	0.40	0.40	0.35	0.35
With IGV ($\gamma = 0^0$)	0.76	0.79	0.59	0.36	0.38	0.39
With IGV ($\gamma = 5^0$)	0.82	0.81	0.41	0.38	0.39	0.36

Table 1b. 'ψ' for various configurations.

	C. I. $\phi = 0.45$	S. M. $\phi = 0.45$	D. M. $\phi = 0.45$	C. I. $\phi = 0.285$	S. M. $\phi = 0.285$	D. M. $\phi = 0.285$
Without IGV	0.32	0.32	0.26	0.19	0.20	0.27
With IGV ($\gamma = -10^0$)	0.39	0.43	0.22	0.24	0.23	0.25
With IGV ($\gamma = 0^0$)	0.35	0.35	0.27	0.19	0.20	0.25
With IGV ($\gamma = 5^0$)	0.32	0.33	0.16	0.18	0.19	0.21

Table 1c. 'P_{coeff}' for various configurations.

	C. I. $\phi = 0.45$	S. M. $\phi = 0.45$	D. M. $\phi = 0.45$	C. I. $\phi = 0.285$	S. M. $\phi = 0.285$	D. M. $\phi = 0.285$
Without IGV	0.18	0.18	0.17	0.13	0.14	0.16
With IGV ($\gamma = -10^0$)	0.24	0.24	0.25	0.16	0.17	0.19
With IGV ($\gamma = 0^0$)	0.21	0.20	0.21	0.14	0.15	0.17
With IGV ($\gamma = 5^0$)	0.18	0.19	0.17	0.13	0.13	0.16

Table 2. Distortion Indices for various configurations.

	Rotor Inlet $\phi = 0.45$	Rotor Exit $\phi = 0.45$	Stator Exit $\phi = 0.45$	Rotor Inlet $\phi = 0.285$	Rotor Exit $\phi = 0.285$	Stator Exit $\phi = 0.285$
Without IGV	1.71	0.79	0.49	1.69	-0.13	0.52
With IGV ($\gamma = -10^0$)	1.62	0.33	0.20	1.57	-0.12	0.40
With IGV ($\gamma = 0^0$)	1.72	0.70	0.46	1.48	-0.13	0.43
With IGV ($\gamma = 5^0$)	1.59	0.32	0.28	1.54	0.052	0.35

CONCLUSIONS

Circumferential distortion causes a reduction in η and ψ of the stage at $\phi = 0.45$ corresponding to the rising portion of the clean performance characteristic. Circumferential distortion causes an increase in ψ and P_{coeff} of the stage at $\phi = 0.285$. The presence of swirl in addition to distortion causes an increased reduction of η and ψ at $\phi = 0.45$ and an increase in ψ at $\phi = 0.285$.

Distortion attenuation was high at the rotor exit for $\phi = 0.285$ due to better redistribution. The defect at the rotor exit is amplified at the stator exit for $\phi = 0.285$ due to higher losses in the stator which result from the increased positive incidences at the inlet to the stator. The overall stage attenuation was high for $\phi = 0.45$. The presence of swirl in addition to distortion caused increased attenuation at the rotor and stator exits for both flow coefficients.

REFERENCES

Aulehla, F., 1982, "Intake Swirl - a Major Disturbance Parameter in Engine/Intake Compatibility," ICAS-82-4.8.1.

Colpin, J., 1979, "Propagation of Inlet Flow Distortions through an Axial Compressor Stage," ASME Journal of Engineering for Power, Vol. 101, pp. 116-124.

Ehrich, F., 1957, "Circumferential Inlet Distortions in Axial Flow Turbomachinery," Journal of the Aeronautical Sciences, Vol. 24, No. 6, pp. 413-417.

Flitcroft, J.E., Dunham, J., and Abbott, W.A., 1987, "Transmission of Inlet Distortion through a Fan," Engine Response to Distorted Inflow Conditions, AGARD CP-400.

Pazur, W., and Fottner, L., 1991, "The Influence of Inlet Swirl Distortions on the Performance of a Jet Propulsion Two Stage Axial Compressor," ASME Journal of Turbomachinery, Vol. 113, pp. 233-240.

Yocum, A.M., and Henderson, R.E., 1980, "The Effects of Some Design Parameters of an Isolated Rotor on Inlet Flow Distortions," ASME Journal of Engineering for Power, Vol. 102, pp. 178-186.